Deep-Red Electroluminescent Polymers: Synthesis and Characterization of New Low-Band-Gap Conjugated Copolymers for Light-Emitting Diodes and Photovoltaic Devices

Renqiang Yang, Renyu Tian, Jingai Yan, Yong Zhang, Jian Yang, Qiong Hou, Wei Yang, Chi Zhang, and Yong Cao*

Institute of Polymer Optoelectronic Materials and Devices, Key Laboratory of Special Functional Materials and Advanced Manufacturing Technology, South China University of Technology, Guangzhou 510640, China

Received October 2, 2004; Revised Manuscript Received November 3, 2004

ABSTRACT: A novel series of semiconducting conjugated copolymers, derived from alkyl-substituted fluorene, 4,7-diselenophen-2′-yl-2,1,3-benzothiadiazole (SeBT), and 4,7-diselenophen-2′-yl-2,1,3-benzoselenadiazole (SeBSe), was synthesized by a palladium-catalyzed Suzuki coupling reaction with various feed ratios. The optical band gap of copolymers is very low, 1.87 eV for SeBT and 1.77 eV for SeBSe. The efficient fast energy transfer from fluorene segments to narrow-band-gap sites was observed. The emission of photoluminescence and electroluminescence is dominated by narrow-band-gap species and peaked at 670−790 nm, in the range from deep-red to near-infrared (NIR). The external electroluminescent (EL) quantum efficiencies reached 1.1% and 0.3% for devices from these two types of copolymers, respectively. Bulk−heterojunction polymer photovoltaic cells (PPVCs) made from composite thin film of the copolymer 9,9-dioctylfluorene and SeBT (PFO−SeBT) in blend with fullerene derivative [6,6]-phenyl C_{61} butyric acid methyl ester (PCBM) as an active layer show promising performances. The energy conversion efficiency (ECE) is up to 1% under AM1.5 solar simulator (78.2 mW/cm^2). The spectral response is extended up to 675 and 750 nm for PPVCs from PFO−SeBT and PFO−SeBSe, respectively.

Introduction

Electroluminescent polymers are a subject of considerable academic and commercial interest when used as the active materials in polymer light-emitting diodes (PLEDs).[1,2] $\pi-\pi^*$ transitions of conjugated polymers with aromatic or heterocyclic units generally lead to the optical band gap with an absorption peak of 300−600 nm.[3] The color purity, quantum efficiency (QE) of light emission, turn-on voltage, and stability of the devices must be optimized for PLEDs to be applicable to commercial light-emitting devices. A large number of electroactive and photoactive conjugated polymers have been introduced during the past few years,[2a] such as poly(*p*-phenylenevinylene) (PPV),[1a,4] poly(*p*-phenylene) (PPP),[5] polythiophene (PT),[6] and polyfluorene (PF),[7] etc. Among those polymers, PLEDs based on polyfluorenes have emerged as a promising candidate for the next generation of flat panel displays[2b,8] because of their exceptional optoelectronic properties, such as good thermal and chemical stability, high fluorescence quantum yield, and good film-forming and hole-transporting properties.[7] Normally, polyfluorene homopolymers have a large band gap and emit blue light. Significant efforts and great success have been made to tune the light-emitting color of polyfluorenes to a longer wavelength.[2b,9−12] However, these efforts were limited to the visible region (500−650 nm). It will be of great interest to extend the emission wavelength to the deep-red and even to the near-infrared (NIR) region to apply these light-emitting polymers to telecommunications.[13] Near-IR-emitting devices with around 800 nm emission have been reported for ionic laser dyes.[14] More efforts have been devoted to complexes from rare-earth ions.[15] On the other hand, conjugated polymers with a small band gap are needed for polymer photovoltaic cells (PPVCs) being used for solar cells. One of the limiting factors of polymer photovoltaic cells is their spectral response mismatching with the solar-terrestrial radiation, which comprises a substantial portion of emission in the red and near-infrared. For a typical conjugated polymer used for PPVCs, poly(2-methoxy-5-(2′-ethylhexyloxy)-1,4-phenylenevinylene) (MEH−PPV), the onset and maximum of its optical absorption are estimated at 590 and 510 nm, respectively. Recently, Brabec et al. reported a low-band-gap alternating copolymer *N*-dodecyl-2,5-bis(2′-thienyl)pyrrole and 2,1,3-benzothiadiazole (PTPTB) which has a band gap of around 1.77 eV.[16]

Color tuning to the deep-red and NIR region in conjugated polymers can be achieved by incorporating narrow-band-gap comonomer into polyfluorene backbone. Recently, we first reported a polyfluorene copolymer with selen-containing heterocycle, benzoselenadiazole (BSeD), a selenium analogue of benzothiadiazole (BT) in different compositions.[11] We found out that incorporating Se-containing heterocycle (BSeD) into the polyfluorene main chain resulted in a significant red shift in comparison with its sulfur analogue. We also reported the synthesis and properties of the polyfluorene copolymer with another selen-containing heterocycle, 2,1,3-naphthoselenadiazole (NSeD) as the narrow band-gap component.[12] The maximal EL external quantum efficiency of the device fabricated with this type of copolymer reaches 3.1%, and luminous efficiency is of 0.9 cd/A with an emission peak at 657 nm and Commission International de l'Eclairage (CIE) coordinates of (0.64, 0.33). These results indicate that synthesizing selen-containing heterocycles with a narrower band gap moves the absorption band edge to a further deep-red or even NIR region without using the metallic complex ions.

* To whom correspondence should be addressed. Phone: +86-20-87114609. Fax: +86-20-87114535. E-mail: poycao@scut.edu.cn.

10.1021/ma047969i CCC: $30.25
Published on Web 12/21/2004

Scheme 1. Synthetic Route of Monomers and Copolymers

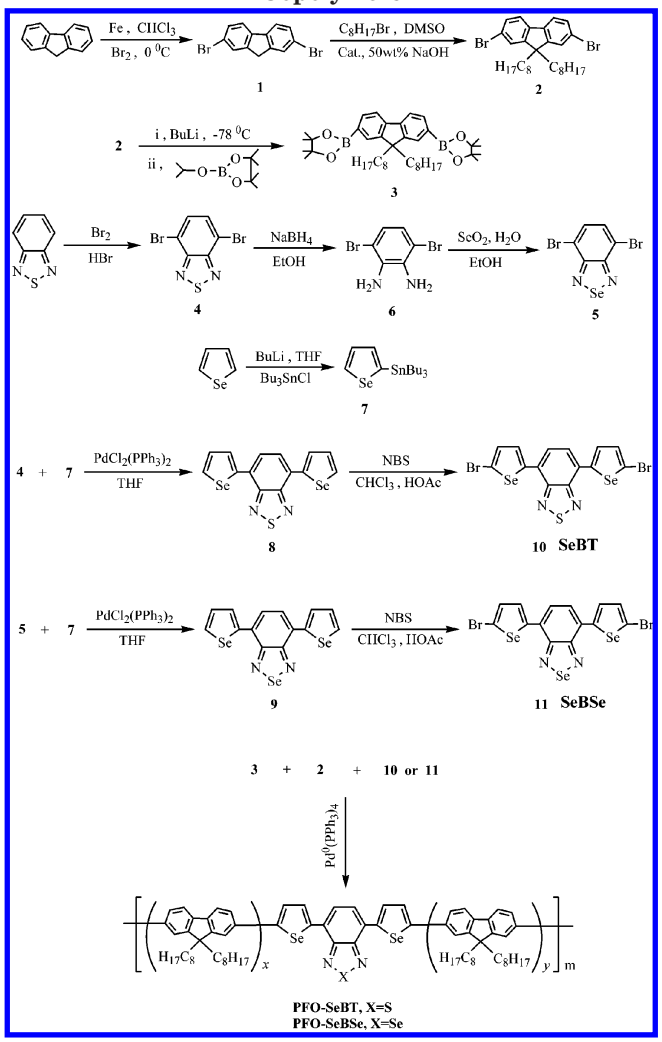

This paper reports the syntheses of two new conjugated Se-containing heterocyclic monomers, 4,7-di(2′-selenophenyl)-2,1,3-benzothiadiazole (SeBT) and 4,7-di(2′-selenophenyl)-2,1,3-benzoselenadiazole (SeBSe) (Scheme 1), which have a narrower band gap than benzoselenadiazole and naphthoselenadiazole. A series of novel copolymers derived from 9,9-dioctylfluorene (FO) and the two Se-containing monomers were prepared by the palladium-catalyzed Suzuki cross-coupling reaction. The feed ratio of the narrow-band-gap component is less than or equal to a molar ratio of 50%. The light-emitting devices and photovoltaic devices were fabricated from the obtained copolymers, the highest external quantum efficiency of the device based on the copolymer PFO−SeBT reaching 1.1% ph/el with an emission peak of ca. 700 nm. The device with PFO−SeBSe emits light with a maximal wavelength of 790 nm in the near-infrared region. The complete synthetic details and device characteristics are presented. The photovoltaic cells made from composite thin films of the copolymer PFO−SeBT blending with the fullerene derivative [6,6]-phenyl C_{61} butyric acid methyl ester (PCBM) as an active layer show promising performances. The energy conversion efficiency (ECE) is up to 1% under AM1.5 solar simulator (78.2 mW/cm^2). The spectral response is extended to 750 nm for devices from blend with PFO−SeBSe copolymers.

Experimental Section

Materials and Characterization. All manipulations involving air-sensitive reagents were performed in an atmosphere of dry argon. All reagents, unless otherwise specified, were obtained from Aldrich, Acros, and TCI Chemical Co. and used as received. All the solvents were further purified before use. ^{1}H and ^{13}C NMR spectra were recorded on a Bruker DRX 400 spectrometer operating, respectively, at 400 and 100 MHz and were referred to tetramethylsilane. Analytical GPC was obtained using a Waters GPC 2410 in tetrahydrofuran (THF) via a calibration curve of polystyrene standards. Elemental analyses were performed on a Vario EL Elemental Analysis Instrument (Elementar Co.). The elemental selenium analysis was recorded on a Polarized Zeeman Atomic Absorption Spectrophotometer, Hitachi Co. UV−visible absorption spectra were measured on a HP 8453 spectrophotometer. The PL quantum yields were determined in an integrating sphere under 405 nm excitation of a laser diode (CL-2000, Crystal Laser). PL and EL spectra were recorded on an Instaspec 4 CCD spectrophotometer (Oriel Co.). Cyclic voltammetry was measured on a Potentiostat/Galvanostat model 283 electrochemical workstation (Princeton Applied Research) at a scan rate of 50 mV/s with a nitrogen-saturated solution of 0.1 M tetrabutylammonium hexafluorophosphate (Bu_4NPF_6) in acetonitrile (CH_3CN) with platinum and saturated calomel electrodes (SCE) as the working and reference electrodes, respectively.

Synthesis. *2,7-Dibromofluorene (**1**) and 2,7-Dibromo-9,9-dioctylfluorene (**2**).* **1** and **2** were prepared following the procedure described in ref 17. **1**: white crystal, yield 93%, mp 161−163 °C. **2**: white crystal, yield 85%, mp 49−50 °C.

*2,7-Bis(4,4,5,5-tetramethyl-1,3,2-dioxaborolan-2-yl)-9,9-dioctylfluorene (**3**).* **3** was prepared following the modified procedure from 2,7-dibromo-9,9-dioctylfluorene (**2**).[18] White solid, yield 79%, mp128−130 °C. ^{1}H NMR (400 MHz, $CDCl_3$) δ (ppm): 7.80 (d, 2H, fluorene ring), 7.74 (s, 2H, fluorene ring), 7.71 (d, 2H, fluorene ring), 1.99 (m, 4H, H-alkyl), 1.39 (s, 24H, CH_3), 1.22−1.00 (m, 20H, H-alkyl), 0.81 (t, 6H, H-alkyl), 0.56 (m, 4H, H-alkyl). ^{13}C NMR (100 MHz, $CDCl_3$) δ (ppm): 150.86, 144.30, 134.04, 129.29, 119.77 (fluorene ring), 84.11 (C-alkyl), 55.57 (C_9, fluorene ring), 40.49, 32.18, 30.33, 29.58, 25.33, 23.98, 22.99, 14.48 (C-alkyl). Anal. Calcd for $C_{41}H_{64}O_4B_2$: C, 76.74; H, 10.04. Found: C, 76.68; H, 9.94).

*4,7-Dibromo-2,1,3-benzothiadiazole (**4**).*[19] A mixture of 13.6 g (0.1 mol) of 2,1,3-benzothiadiazole in 30 mL of 45% hydrobromic acid was heated under reflux with stirring while 48 g (0.3 mol, 15.3 mL) of bromine was added slowly. After completion of the bromine addition, the reaction mixture became a suspension of solid in hydrobromic acid and 15 mL of hydrobromic acid was added, and the mixture was heated under reflux for another 2.5 h. The mixture was filtered, washed well with water, recrystallized from chloroform, and dried to give white needle crystals (27.3 g, 93%). mp 187−188 °C. ^{1}H NMR (400 MHz, $CDCl_3$) δ (ppm): 7.73 (s, 2H). ^{13}C NMR (100 MHz, $CDCl_3$) δ (ppm): 153.34, 132.67, 114.31.

*4,7-Dibromo-2,1,3-benzoselenadiazole (**5**).*[20] To a suspension of 4,7-dibromo-2,1,3-benzothiadiazole (**4**) (5.88 g, 0.02 mol) in ethanol (190 mL) was added portionwise sodium borohydride (14 g, 0.37 mol) at 0 °C, and the mixture was stirred for 20 h at room temperature. After evaporation of the solvent, 200 mL of water was added, and the mixture was extracted with ether. The extract was washed with brine and dried over anhydrous sodium sulfate. Evaporation of the solvent gave 3,6-dibromo-1, 2-phenylenediamine (**6**) (4.5 g) as a pale yellow solid in 85% yield. To a solution of **6** (2.7 g, 10 mmol) in refluxing ethanol (55 mL) was added a solution of selenium dioxide (1.17 g, 10.5 mmol) in hot water (22 mL). The mixture was heated under reflux for 2 h. Filtration of the yellow precipitates and recrystallization from ethyl acetate gave 4,7-dibromo-2,1,3-benzoselenadiazole (**5**) (3.0 g) in 88% yield as golden yellow needles. mp 285−287 °C. ^{1}H NMR (400 MHz, $CDCl_3$) δ (ppm): 7.63 (s, 2H, phenylene ring). ^{13}C NMR (100 MHz, $CDCl_3$) δ (ppm): 157.2, 132.1, 116.5. Anal. Calcd for $C_6H_2Br_2N_2Se$: C, 21.1; H, 0.6; N, 8.2. Found: C, 21.4; H, 0.9; N, 7.8.

*Tributyl(2-selenophenyl)stannane (**7**).* **7** was prepared following the modified published procedures.[21] *n*-Butyllithium (22 mL of a 2.0 M solution in hexane, 44 mmol) was added dropwise to selenophene (10 g, 76.4 mmol) in anhydrous tetrahydrofuran (70 mL) at −30 °C, and the mixture was stirred at this temperature under argon for 3.5 h. Tributyltin chloride (13.02 g, 40 mmol) was added, and the mixture was stirred at −30 °C for a further 1 h. Saturated aqueous sodium hydrogen carbonate (70 mL) was added, and the organic phase was separated and washed with saturated aqueous sodium hydrogen carbonate (70 mL) and brine (40 mL). The solvent was evaporated from the dried sodium sulfate extract, and the residue was purified by column chromatography on neutral alumina (eluent petroleum ether) to give the title compound **7** (10.2 g, 61%) as colorless oil without further purification for the next step synthesis. *m/z*, 419.6.

*4,7-Diselenophen-2′-yl-2,1,3-benzothiadiazole (**8**).*[22] To a solution of 4,7-dibromo-2,1,3-benzothiadiazole (**4**) (1.45 g, 4.9 mmol) and tributyl(2-selenophenyl)stannane (**7**) (5.0 g, 11.9 mmol) in anhydrous THF (30 mL), $PdCl_2(PPh_3)_2$ (70 mg, 2 mol %) was added. The mixture was refluxed for 4 h. After removal of the solvent under reduced pressure, the residue was purified by column chromatography on silica gel (eluent CH_2Cl_2/hexane, 1:1). Recrystallization from toluene−ethanol gave the title compound **8** (1.45 g, 75%) as red needles. *m/z*, 394.

*4,7-Diselenophen-2′-yl-2,1,3-benzoselenadiazole (**9**).* **9** was prepared according to the modified procedure for the synthesis of compound **8**. 4,7-Dibromo-2,1,3-benzoselenadiazole (**5**) (1.77 g, 5.2 mmol), tributyl(2-selenophenyl)stannane (**7**) (5.2 g, 12.4 mmol), and $PdCl_2(PPh_3)_2$ (74 mg, 2 mol %) were dissolved in 35 mL of anhydrous THF. The mixture was refluxed for 4.5 h. After removal of the solvent under reduced pressure, the residue was purified by column chromatography on silica gel (eluent CH_2Cl_2/hexane, 1:1). Recrystallization from toluene−ethanol gave the title product **9** (1.74 g, 76%) as dark red needles. *m/z*, 441.

*4,7-Bis(5′-bromo-2′-selenophenyl)-2,1,3-benzothiadiazole (SeBT) (**10**).*[9] 4,7-Diselenophen-2′-yl-2,1,3-benzothiadiazole (**8**) (1.45 g, 3.7 mmol) was dissolved in a mixture of chloroform (30 mL) and acetic acid (30 mL) under nitrogen, and *N*-bromosuccinimide (1.4 g, 7.8 mmol) was added all at once. After stirring the reaction mixture at room temperature all night, the red precipitate was filtered off and recrystallized from *N*,*N*-dimethylformamide (DMF) twice to provide the title compound as shiny, red crystals (0.84 g, 41%). FAB, 552. mp 225−230 °C. ^{1}H NMR (400 MHz, $CDCl_3$) δ (ppm): 8.15, 7.98, 7.52. Anal. Calcd for $C_{14}H_6Br_2N_2S_1Se_2$: C, 30.46; H, 1.10; N, 5.07; S, 5.81; Se, 28.61. Found: C, 30.39; H, 1.16; N, 5.16; S, 5.90; Se, 28.86.

*4,7-Bis(5′-bromo-2′-selenophenyl)-2,1,3-benzoselenadiazole (SeBSe) (**11**).* **11** was made following the modified procedure for the preparation of compound **10**. 4,7-Diselenophen-2′-yl-2,1,3-benzoselenadiazole (**9**) (1.74 g, 4.0 mmol) was dissolved in a mixture of chloroform (30 mL) and acetic acid (30 mL) under nitrogen, and *N*-bromosuccinimide (1.5 g, 8.4 mmol) was added all at once. After stirring the reaction mixture for 24 h at room temperature, the dark red precipitate was filtered off and recrystallized from DMF to give the title product as shiny, dark red needle crystals (0.86 g, 36%). FAB, 599. mp 235−239 °C. ^{1}H NMR (400 MHz, $CDCl_3$) δ (ppm): 8.17, 8.02, 7.54. Anal. Calcd for $C_{14}H_6Br_2N_2Se_3$: C, 28.08; H, 1.01; N, 4.68; Se, 39.54. Found: C, 27.96; H, 1.10; N, 4.59; Se, 39.25.

General Procedure for Polymer Synthesis.[23] Carefully purified 2,7-dibromo-9,9-dioctylfluorene (**2**), 2,7-bis(4,4,5,5-tetramethyl-1,3,2-dioxaborolan-2-yl)-9,9-dioctylfluorene (**3**), 4,7-bis(5′-bromo-2′-selenophenyl)-2,1,3-benzothiadiazole (**SeBT**) (**10**), or 4,7-bis(5′-bromo-2′-selenophenyl)-2,1,3-benzoselenadiazole (**SeBSe**) (**11**), $(PPh_3)_4Pd(0)$ (0.5−2.0 mol %), and several drops of Aliquat 336 were dissolved in a mixture of toluene and aqueous 2 M Na_2CO_3 with THF as a cosolvent. The solution was refluxed with vigorous stirring for 36 h under an argon atmosphere. At the end of polymerization, polymers were sequentially end-capped with 2,7-bis(4,4,5,5-tetramethyl-1,3,2-dioxaborolan-2-yl)-9,9-dioctylfluorene and bromobenzene to remove bromine and boronic ester end groups in order to avoid a possible quenching effect or excimer formation by boronic and bromine end groups in LEDs.[24] The mixture was then poured into methanol. The precipitated material was recovered by filtration and washed for 3 h by stirring in acetone to remove oligomers and catalyst residues. The resulted polymers were air-dried overnight, followed by drying under vacuum. Yields: ∼55−80%.

Poly[2,7-(9,9-dioctylfluorene)-co-5′,5″-(4,7-diselenophen-2′-yl)-2,1,3-benzothiadiazole] (PFO−SeBT). The ratio of 2,7-bis-(4,4,5,5-tetramethyl-1,3,2-dioxaborolan-2-yl)-9,9-dioctylfluorene (**3**) (1.00 equiv) vs dibromides (2,7-dibromo-9,9-dioctylfluorene (**2**) and 4,7-bis(5′-bromo-2′-selenophenyl)-2,1,3-benzothiadiazole (**10**)) was kept always as (**2**+**10**):(**3**)= 1:1. The comonomer feed ratios of (**2**+**3**) to **10** are 99:1, 95:5, 90:10, 85:15, 70:30, and 50:50, and the corresponding copolymers were named PFO−SeBT1, -5, -10, -15, -30, and -50, respectively.

Poly[2,7-(9,9-dioctylfluorene)-co-5′,5″-(4,7-diselenophen-2′-yl)-2,1,3-benzoselenadiazole] (PFO−SeBSe). In this polymerization 2,7-bis(4,4,5,5-tetramethyl-1,3,2-dioxaborolan-2-yl)-9,9-dioctylfluorene (**3**) (1.00 equiv) and dibromides 2,7-dibromo-9,9-dioctylfluorene (**2**) and 4,7-bis(5′-bromo-2′-selenophenyl)-2,1,3-benzoselenadiazole (**11**) (1.00 equiv of **2**+**11**) were used. The comonomer feed ratios of (**2**+**3**) to **11** are 99:1, 95:5, 90:10, and 85:15, and the corresponding copolymers were named PFO−SeBSe1, -5, -10, and -15, respectively.

Device Fabrication and Characterization. LED was fabricated on prepatterned indium−tin oxide (ITO) with a sheet resistance 10−20 Ω/□. The substrate was ultrasonically cleaned with acetone, detergent, deionized water, and 2-propanol subsequently. Oxygen plasma treatment was made for 10 min as the final step of substrate cleaning to improve the contact angle just before film coating. Onto the ITO glass a layer of polyethylenedioxythiophene−polystyrene sulfonic acid (PEDT:PSS) film with a thickness of 50 nm was spin coated from its aqueous dispersion (Baytron P 4083, Bayer AG), aiming to improve the hole injection and avoid the possibility of leakage. PEDT−PSS film was dried at 80 °C for 2 h in the vacuum oven. The solution of the copolymers in toluene was prepared in a nitrogen-filled drybox and spin coated on top of the ITO/PEDT:PSS surface. The typical thickness of the emitting layer was 70−80 nm. Then a thin layer of barium as an electron injection cathode and the subsequent 200-nm thick aluminum capping layers were thermally deposited by vacuum evaporation through a mask at a base pressure below 2×10^{-4} Pa. The deposition speed and thickness of the barium and aluminum layers were monitored by a thickness/rate meter, model STM-100 (Sycon Instrument, Inc.). The cathode area defines the active area of the device. The typical active area of the devices in this study is 0.15 cm^2. The spin coating of the EL layer and device performance tests were carried out within a glovebox (Vacuum Atmosphere Co.) with nitrogen circulation. Current−voltage (*I*−*V*) characteristics were measured with a computerized Keithley 236 Source Measure Unit. The luminance of the device was measured with a photodiode calibrated by using a PR-705 SpectraScan Spectrophotometer (Photo Research). External quantum efficiency was verified by measurement in the integrating sphere (IS080, Labsphere) after encapsulation of devices with UV-curing epoxy and thin cover glass.

Results and Discussion

Synthesis and Chemical Characterization. The general synthetic routes toward the monomers are outlined in Scheme 1. 2,7-Dibromo-9,9-dioctylfluorene (**2**) and 2,7-bis(4,4,5,5-tetramethyl-1,3,2-dioxaborolan-2-yl)-9,9-dioctylfluorene (**3**) were synthesized by published procedures.[17,18] 4,7-Bis(5′-bromo-2′-selenophenyl)-2,1,3-benzothiadiazole (**10**) and 4,7-bis(5′-bromo-2′-selenophenyl)-2,1,3-benzoselenadiazole (**11**) were prepared following the modified procedures in the literature.[9,19−22] Following the polymer synthetic route in Scheme 1, the conjugated copolymers derived from 2,7-dibromo-9,9-dioctylfluorene (**2**) and 2,7-bis(4,4,5,5-tet-

Table 1. Molecular Weights of the Copolymers and N and Se Content in the Copolymers

copolymers	M_n (10^3)	M_w/M_n	N content in the feed composition (%)	N content in the copolymers (%)	Se content in the feed composition (%)	Se content in the copolymers (%)	SeBT or SeBSe content in the copolymers (%) according to N content	SeBT or SeBSe content in the copolymers (%) according to Se content
PFO-SeBT1	21	1.60	0.07	<0.2	0.41	0.38		0.94
PFO-SeBT5	28	1.43	0.36	0.30	2.03	1.93	4.2	4.7
PFO-SeBT10	25	2.01	0.72	0.67	4.07	3.74	9.3	9.2
PFO-SeBT15	24	1.59	1.08	1.18	6.10	6.31	16.3	15.5
PFO-SeBT30	12	1.78	2.16	2.02	12.17	11.31	28.1	27.9
PFO-SeBT50	8	1.51	3.59	3.17	20.25	17.50	44.2	43.2
PFO-SeBSe1	23	1.86	0.07	<0.2	0.61	0.58		0.95
PFO-SeBSe5	20	1.83	0.36	0.31	3.03	2.81	4.3	4.6
PFO-SeBSe10	28	1.95	0.71	0.64	6.03	5.31	9.0	8.8
PFO-SeBSe15	13	1.72	1.06	0.97	8.98	7.79	13.7	13.0

Table 2. UV−Vis Absorption and Electrochemical Properties of the Copolymers in Thin Films

copolymers	λ_{max}, UV/nm	optical band gap/eV[a]	E_{ox}/V[b]	E_{red}/V[b] PFO, SeBT/SeBSe	HOMO/eV[c]	LUMO/eV[c] PFO, SeBT/SeBSe	$E_{g(Echem)}$/eV PFO, SeBT/SeBSe
PFO	382	2.92 (424)	1.37	−2.24	−5.77	−2.16	3.61
PFO-SeBT1	383	2.92(424)	1.30	−2.27	−5.70	−2.13	3.57
PFO-SeBT5	384, 561	1.88 (658)	1.30	−2.31	−5.70	−2.09	3.61
PFO-SeBT10	385, 563	1.88 (661)	1.28	−2.30	−5.68	−2.10	3.58
PFO-SeB T15	387, 563	1.87 (664)	1.20	−2.23	−5.60	−2.17,	3.43
PFO-SeBT30	389, 560	1.85 (670)	1.11	−2.19, −1.64	−5.51	−2.76	3.30, 2.75
PFO-SeBT50	385, 537	1.89 (656)	1.28	−2.44, −1.61	−5.68	−2.79	3.72, 2.89
PFO-SeBSe1	382	2.92 (425)	1.33	−2.29	−5.73	−2.11,	3.62
PFO-SeBSe5	380, 604	1.78 (696)	1.31	−2.23	−5.71	−2.17,	3.54
PFO-SeBSe10	385, 609	1.77 (700)	1.31	−2.12	−5.71	−2.28,	3.43
PFO-SeBSe15	393, 585	1.78 (695)	1.13	−2.17, −1.47	−5.53	−2.93	3.30, 2.60

[a] The optical band gap estimated from the onset wavelength (value in parentheses) of UV−vis spectra of the copolymer film. [b] E_{ox} and E_{red} are the onset potential of oxidation and reduction, respectively. [c] Calculated from the empirical formula, $E_{(HOMO)} = -(E_{ox} + 4.40)$ (eV), $E_{(LUMO)} = -(E_{red} + 4.40)$ (eV).[26]

ramethyl-1,3,2-dioxaborolan-2-yl)-9,9-dioctylfluorene (**3**) were synthesized separately with monomers **10** and **11** using the palladium-catalyzed Suzuki coupling method. The obtained copolymers are completely soluble in common organic solvents, such as toluene, THF, and chloroform. The number-average molecular weights of these polymers, as determined by GPC using a polystyrene standard, ranged from 8000 to 28 000 with a polydispersity index (M_w/M_n) between 1.43 and 2.01 (Table 1).

The actual ratios of substituted fluorene to narrow-band-gap monomer in the copolymers can be estimated by elemental analysis. The selenium contents of these polymers were measured by atomic absorption spectroscopy. The actual ratios calculated from elemental analysis of Se or N and C are listed in Table 1, which is in good agreement with the feeding ratios of the two monomers within experimental error. Slightly larger deviation for copolymers PFO−SeBT30, PFO−SeBT50, and PFO−SeBSe15 calculated from the Se content might be due to a larger error of the atomic absorption spectroscopy for the samples with high Se content.

The chemical structure of the PFO−SeBT and PFO−SeBSe copolymer was verified by ^{1}H and ^{13}C NMR. For example, in the proton NMR spectra, the characteristic signal of the benzene proton in benzothiadiazole can be seen clearly at around δ 8.2−8.4 ppm (depending on SeBT content) for all copolymers with SeBT content equal to or greater than 5% molar ratio of SeBT. The integration intensity of this signal increases with increasing the SeBT content in comparison with the fluorene proton at around δ 7.70 ppm. The low-field carbon NMR signal at around δ 152.6 ppm, which can be assigned to carbon in the benzothiadiazole ring, can be clearly seen for all copolymers. Similar results were observed for the NMR spectra of PFO−SeBSe copolymers.

Optical Properties and Electrochemical Characteristics. The UV−vis absorption properties of the conjugated polymers based on 9,9-dioctylfluorene, SeBT, and SeBSe are presented in Table 2. Figure 1 shows the normalized UV−vis absorption of the polymers in the thin solid films (Figure 1a and c) and in chloroform solution (5×10^{-5} mol/L) (Figure 1b and d). Two distinct absorption bands are observed. The absorption peak of 385 nm is due to the fluorene segments compared with the absorption spectrum of pure poly(9,9-dioctylfluorene) (PFO).[11,25] A side peak of about 563 nm can be assigned to the absorption of the SeBT unit (Figure 1a), since its intensity increases with the increasing SeBT content in the copolymers. For the PFO−SeBT50 copolymer, the shoulder is about 20 nm more blue shifted than that of PFO−SeBT30, which is probably due to band alternation. For the PFO−SeBSe copolymers (Figure 1c), the intensities of the shoulder peak at about 605 nm increase linearly with the SeBSe content, suggesting that the 605 nm absorption band originated from SeBSe units. Two distinguished absorption features demonstrate that the electronic states of the two components in copolymers PFO−SeBT and PFO−SeBSe are not mixed. The shoulder peaks are hard to see in the absorption spectra for the copolymers with 1% narrow-band-gap comonomer content. The optical band gaps deducted from the onset of the absorption of copolymers are about 1.87 and 1.77 eV for PFO−SeBT and PFO−SeBSe copolymers, respectively. Maximal wavelengths of the absorption peak, optical band gaps of the copolymers, and their onset wavelengths are summarized in Table 2.

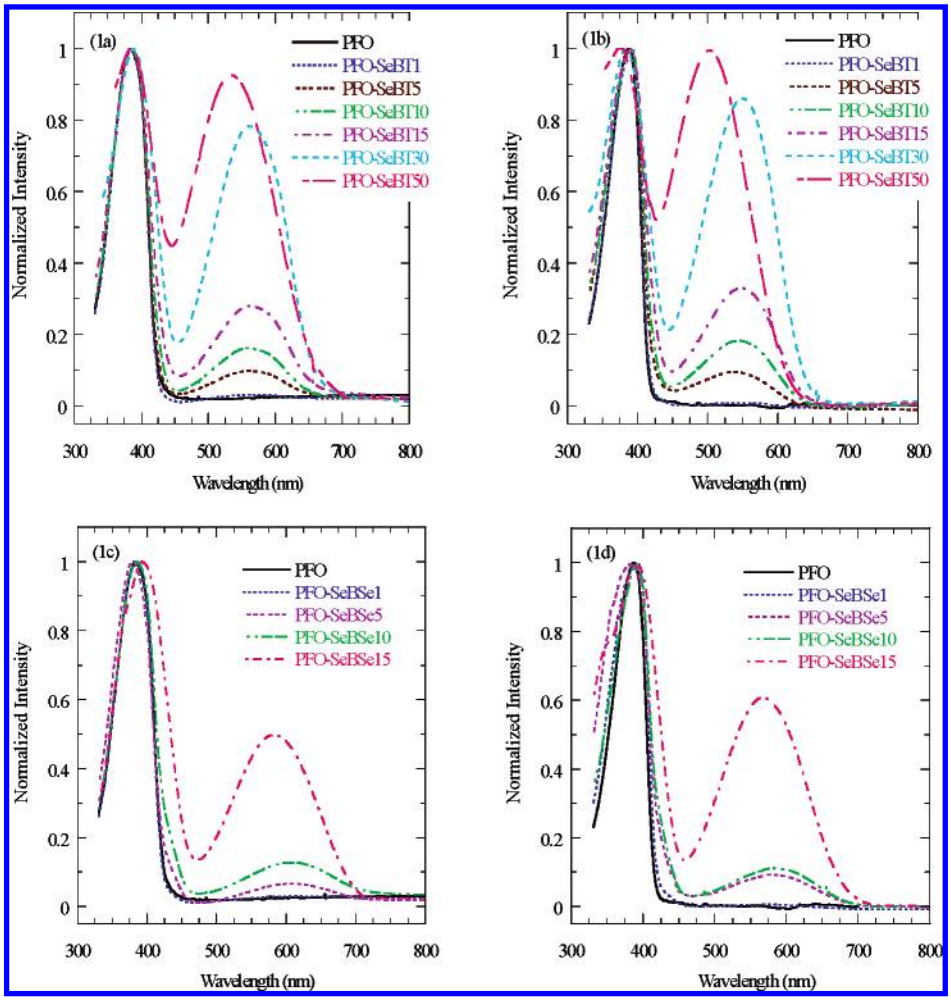

Figure 1. UV−vis absorption spectra of the copolymers (a) PFO−SeBT in the thin films, (b) PFO−SeBT in chloroform solution, (c) PFO−SeBSe in thin films, and (d) PFO−SeBSe in chloroform solution.

The electrochemical behavior of the copolymers was investigated by cyclic voltammetry (CV). Table 2 summarizes the oxidation and reduction potentials derived from the onset of oxidation waves in the cyclic voltammograms of the copolymers. We can record only one p-doping process for these copolymers. The onset potentials of the oxidation process (p-doping) occur at about 1.3 V. The onset of distinct reduction waves (n-doping) occur at about −2.24 V. When the content of SeBT and SeBSe is more than 15%, a second n-doping was recorded. For PFO−SeBT that occurs at −1.61 V and for PFO−SeBSe at −1.47 V. The highest occupied molecular orbital (HOMO) and lowest unoccupied molecular orbital (LUMO) levels of the copolymers can be estimated by the empirical formulas $E_{(\mathrm{HOMO})} = -(E_{\mathrm{ox}} + 4.40)$ (eV) and $E_{(\mathrm{LUMO})} = -(E_{\mathrm{red}} + 4.40)$ (eV).[26] From the differences between the onset potentials of the oxidation and reduction processes, the electrochemical band gaps, $E_{g(\mathrm{Echem})} = (E_{\mathrm{ox}} - E_{\mathrm{red}})$ (eV), of the copolymers were calculated and are listed in Table 2. The oxidation and reduction potentials of the copolymers at about 1.3 and −2.24 V are very close to those reported for the polyfluorene homopolymer: $E_{\mathrm{ox}} = 1.4$ V and $E_{\mathrm{red}} = -2.28$ V.[25] The two peaks are attributed to the p- and n-doping of PFO segments. The reduction waves at about −1.61 and −1.47 V correspond to the n-doping processes on the SeBT and SeBSe units, respectively. The electrochemical behavior of these copolymers is consistent with the two separated absorption peaks observed in the UV−vis spectra (Figure 1). As reported previously by Janietz et al.,[25] the electrochemical band gap for polyfluorene homopolymer is much larger than the optical band gap deducted from the absorption onset, which is due to the existence of an additional interface barrier for charge injection in the electrochemical process.[27]

Photoluminescence Properties. The photoluminescent (PL) spectra of the copolymers (PFO−SeBT and PFO−SeBSe) were taken under excitation of the 405 nm line of the laser diode (CL-2000, Crystal Laser) (Figures 2and 3). PL spectra of PFO homopolymer were included for comparison. Once the narrow-band-gap unit (SeBT or SeBSe) is incorporated into the polyfluorene main chain, the PL emission corresponding to the fluorene segment completely disappeared while the PL emission consists exclusively of one peak at longer wavelength responsible for SeBT and SeBSe units with narrow-band-gap comonomer loading as low as 1% in the copolymer (Figures 2a and 3a). The PL peaks are significantly red shifted with increasing SeBT content in the copolymers, from $\lambda_{\mathrm{max}} = 671$ nm for copolymer with 1% SeBT content to 713 nm for alternating copolymer (Figure 2a and Table 4). For PFO−SeBSe copolymers, the peak of the SeBSe unit emission was shifted from 734 nm for PFO−SeBSe1 to 790 nm for PFO−SeBSe15 (Figure 3a and Table 4). Since no large red shift was observed for absorption spectra of the corresponding copolymers (Figure 1), the significant red shift in PL emission indicates that the Stokes shift increases with the increase in SeBT or SeBSe content

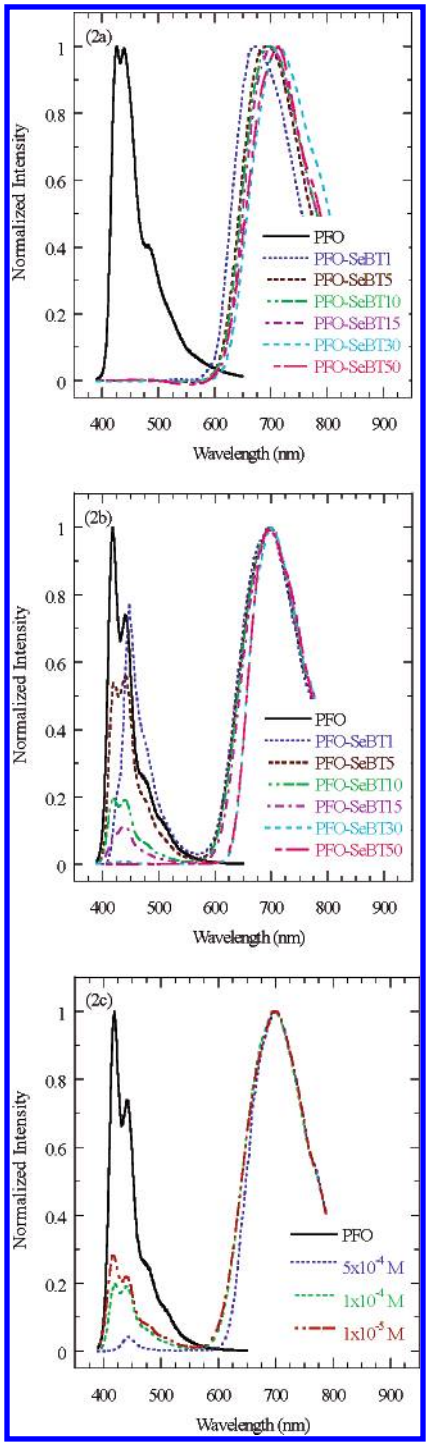

Figure 2. PL spectra of (a) PFO−SeBT copolymers in thin films, (b) PFO−SeBT copolymers in chloroform solution at a concentration of 1×10^{-4} mol/L, and (c) PFO−SeBT10 in chloroform solution in different concentrations.

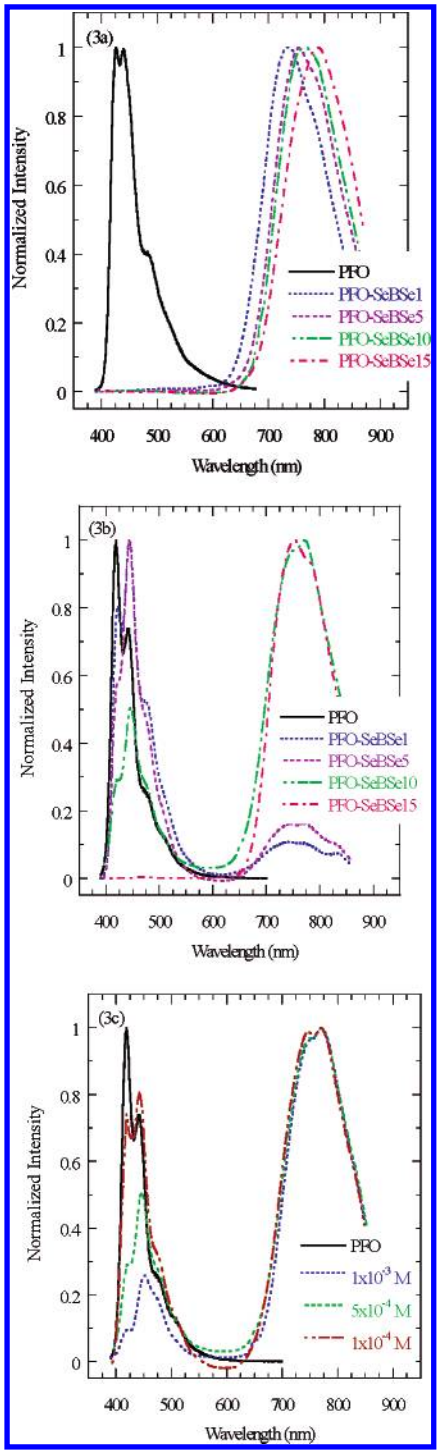

Figure 3. PL spectra of (a) PFO−SeBSe copolymers in thin films, (b) PFO−SeBSe copolymers in chloroform solution at a concentration of 5×10^{-4} mol/L, and (c) PFO−SeBSe10 in chloroform solution in different concentrations.

in the copolymers. The reason for the increase of Stokes shift on increasing narrow-band-gap units in the copolymers is probably due to the higher polarizability of SeBT and SeBSe heterocycles, allowing greater adjustment in the excited state. Similar phenomena were observed for PFO−BSeD copolymers.[11]

The fact that the emission of the fluorene segment completely disappeared at very low loading of narrow-band-gap comonomers indicates that an efficient energy transfer occurs from the fluorene segment to the narrow-band-gap unit, which serves as a powerful trap in the copolymer chain. Excitons are confined and recombined on narrow-band-gap units isolated from both sides by fluorene segment and emit red light corresponding to SeBT or SeBSe unit emission. Energy transfer from fluorene segments to the narrow-band-gap unit may occur via the intra- or intermolecular mechanism. To elucidate the relative role of intra- and interchain energy transfer, we investigated the concentration dependence of PL spectra of the copolymers in chloroform solution. Figure 2b compares the PL spectra of the copolymers with different SeBT contents at a concentration of 1×10^{-4} mol/L (a sufficiently dilute regime to avoid strong intermolecular interaction between poly-

Table 3. Threshold Concentration of Copolymers at Which Fluorescence of Fluorene Segments Is Just Quenched

copolymers	threshold concentration[a] (mol/L)	copolymers	threshold concentration[a] (mol/L)
PFO-SeBT 1	5×10^{-3}	PFO-SeBSe 1	5×10^{-2}
PFO-SeBT 5	1×10^{-3}	PFO-SeBSe 5	5×10^{-3}
PFO-SeBT 10	5×10^{-4}	PFO-SeBSe 10	1×10^{-3}
PFO-SeBT 15	1×10^{-4}	PFO-SeBSe 15	1×10^{-5}
PFO-SeBT 30	1×10^{-5}		
PFO-SeBT 50	1×10^{-7}		

[a] Concentration at which fluorescence of PFO is completely quenched.

Table 4. Comparison of Absolute PL Efficiencies for PFO−SeBT and PFO−SeBSe Copolymers in Thin Films Measured in the Integrating Sphere

	photoluminescence			photoluminescence	
copolymers	λ_{max}/ nm	QE_{PL} (%)	copolymers	λ_{max}/ nm	QE_{PL} (%)
PFO	426	47	PFO	426	47
PFO-SeBT1	671	59	PFO-SeBSe1	734	22
PFO-SeBT5	692	39	PFO-SeBSe5	754	9
PFO-SeBT10	694	16	PFO-SeBSe10	770	9
PFO-SeBT15	697	15	PFO-SeBSe15	790	1
PFO-SeBT30	713	5			
PFO-SeBT50	713	3			

mer chains in the solution). At this relatively dilute concentration copolymers PFO−SeBT30 and PFO−SeBT50 exhibit exclusively SeBT emission while fluorene segment emission was completely quenched. This seems to indicate that the transfer of the exciton energy from fluorene segment to the narrow-band-gap site (SeBT) occurs mainly along the polymer chain. In other words, the efficient energy transfer from fluorene segment to SeBT unit occurs when an intramolecular trapping mechanism takes place.[28,29] However, when the SeBT content was less than 30%, along with the main emission peak in the red region, a small shoulder in the blue region due to fluorene segment emission can be observed in the PL spectra, and its intensity increased with decreasing SeBT content (Figure 2b). Compared with the PL spectra in thin films (Figure 2a), fluorene emission completely disappears for 1% SeBT content. The fact indicates that the energy transfer in such a concentration is incomplete for copolymers with low SeBT content in the solution. We have to note that PFO−SeBT1 has an average molecular weight of 21 000, corresponding to around 54 monomer units per polymer chain (Table 1). Statistically, only one copolymer chain out of two has one SeBT unit. In other words, about one-half of the copolymer chains should be PFO homopolymer in PFO−SeBT1. The interchain energy transfer must take place in the solid-state film in order to quench completely the PL emission from fluorene segment. Figure 2c shows PL spectra of PFO−SeBT10 with different concentrations in chloroform solution. Fluorene segment emission in the copolymer was completely depressed at a concentration of around 5×10^{-4} mol/L. In Table 3 we list the threshold concentration of the solution of each copolymer, where fluorene emission was completely quenched. With increasing SeBT content in the copolymers, the threshold concentration for complete energy transfer decreases. A very low threshold concentration for completed depression of fluorene host emission for PFO−SeBT copolymers seems to suggest that the intramolecular energy transfer is an efficient and quick process and plays a major role in such copolymers in the solution. However, the increase in the threshold concentration with decreasing SeBT content in the copolymer (Table 3) indicates that the interchain energy transfer (interchain interaction) also plays a certain role, especially in copolymers with a low content of narrow-band-gap comonomers.

For PFO−SeBSe copolymers, similar characteristics of the PL spectra in solution were observed (Figure 3b and c). However, there was some difference between the two types of copolymers. Figure 3b shows the PL spectra of PFO−SeBSe copolymers in chloroform solution at a concentration of 5×10^{-4} mol/L. As can be seen from Figure 3b, for copolymers PFO−SeBSe1 and PFO−SeBSe5, the PL spectra are dominated by PFO emission while emission of the SeBSe unit at 760 nm was weak. With increasing the content of SeBSe, the emission at 760 nm becomes gradually dominant. The threshold concentration of PFO−SeBSe in solution for each copolymer was 5−10 times greater than that of the corresponding counterpart of PFO−SeBT (Figure 3c, Table 3). This fact indicates that the interchain interaction between PFO−SeBSe chains is weaker than that of PFO−SeBT copolymer, which is probably related to more rigid chains of PFO−SeBSe because of more Se atoms of larger atomic size in each monomer unit.

In Table 4 we list the absolute PL quantum efficiencies of the copolymers in the thin film measured in an integrating sphere under 405 nm excitation of an UV laser diode (CL-2000, Crystal Laser). For PFO−SeBT copolymers, the PL efficiencies increase with incorporation of a small amount of SeBT unit, reaching 59% and 39% for PFO−SeBT1 and PFO−SeBT5, respectively. With further increases in the SeBT content, the PL efficiencies decrease very quickly, falling to 3% for the alternating copolymers. The initial increase in PL efficiency with incorporation of SeBT content of 1% and 5% molar ratios in the copolymers is probably due to disturbing the regularity of the PFO segments by a big-size Se-containing heterocycle in the copolymer main chains. The further decrease in PL efficiency with the increase in SeBT content is related to the heavy atomic quenching effect by Se atoms. This is consistent with the fact that for PFO−SeBSe copolymers with three Se atoms in each SeBSe comonomer unit there was no initial increase in PL efficiency observed. For PFO−SeBSe1, the PL efficiency decreases to 22%, in comparison with 47% for PFO homopolymers. The PL efficiency of PFO−SeBSe copolymers decreases more rapidly with increasing SeBSe content than for PFO−SeBT copolymers. For PFO−SeBSe15, the PL efficiency decreases to 1%. The heavy-atom effect from the selenium may increase the intersystem crossing from the singlet to triplet state, which quenches fluorescence. The maximum emission wavelengths of the copolymers in thin films are also listed in Table 4. It is worthwhile to note that the emission peaks of PFO−SeBSe copolymers have been shifted to the near-infrared (from 734 nm for PFO−SeBSe1 to 790 nm for PFO−SeBSe15). This is among the longest emission wavelength realized without using rare-earth metal ions or organic dye ions.[16,30,31]

Electroluminescent Properties. The EL properties of the copolymers were investigated using a double-layer device fabricated in the configuration ITO/hole transport layer/polymer/Ba/Al, where the hole transport layer was either PEDT or PEDT/poly(*N*-vinylcarbazole) (PVK). Figure 4 shows the EL spectra from such a device, compared with EL spectra of a device from polyfluorene

Table 5. Device Performances of the Copolymers (ITO/hole transport layer/polymer/Ba/Al)

		device performances[a]				
copolymers	hole transport layer	λ_{ELmax}/nm	QE[b] (%)	L[c]/cd·m^{-2}	current density[d]/mA·cm^{-2}	V[e]/V
PFO-SeBT1	PEDT	661	0.75	85	40.0	9.6
	PEDT/PVK	667	0.67	80	40.0	16.5
PFO-SeBT5	PEDT	676	0.54	60	40.0	8.6
	PEDT/PVK	676	0.81	96	40.0	13.9
PFO-SeBT10	PEDT	682	0.20	23	40.0	8.3
	PEDT/PVK	697	0.50	56	40.0	13.3
PFO-SeBT15	PEDT	687	0.32	37	40.0	4.8
	PEDT/PVK	697	0.70	83	40.0	9.6
PFO-SeBT30	PEDT	712	0.05	6	40.0	5.6
	PEDT/PVK	708	0.15	17	40.0	7.8
PFO-SeBT50	PEDT	708	0.02	2	40.0	8.4
	PEDT/PVK	708	0.02	2	40.0	9.0
PFO-SeBSe1	PEDT	723	0.23	26	40.0	11.4
	PEDT/PVK	723	0.30	38	40.0	16.7
PFO-SeBSe5	PEDT	749	0.05	5	40.0	9.4
	PEDT/PVK	744	0.05	6	40.0	21.2
PFO-SeBS e10	PEDT	759	0.11	13	40.0	11.5
	PEDT/PVK	759	0.20	24	40.0	17.7
PFO-SeBSe15	PEDT	790	0.01	1	40.0	8.6
	PEDT/PVK	790	0.02	2	40.0	9.7

[a] Device structure: ITO/hole transport layer/polymer/Ba/Al, active area 0.15 cm^2. [b] External quantum efficiency. [c] Luminance. [d] Current density. [e] Operating voltage at 40 mA/cm^2.

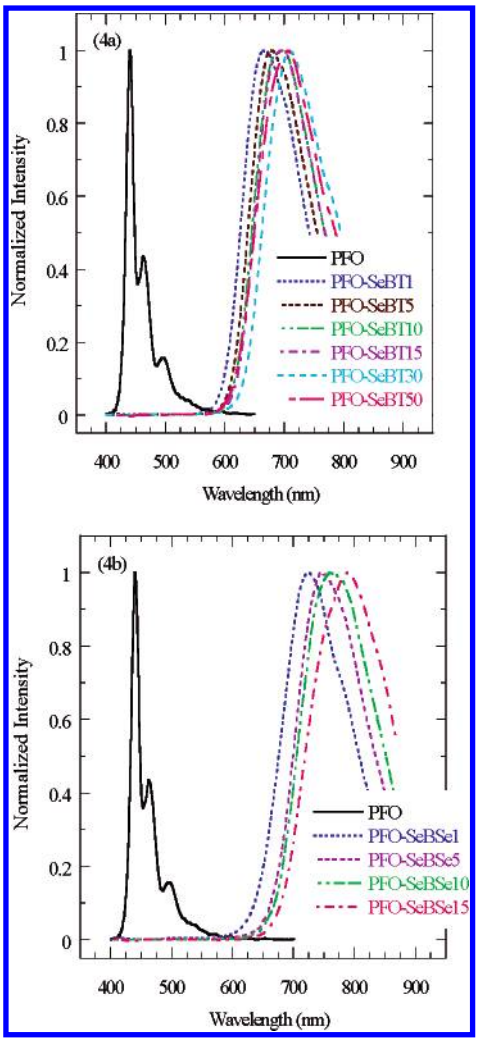

Figure 4. EL spectra of (a) PFO−SeBT copolymers and (b) PFO−SeBSe copolymers in device configuration: ITO/PEDT/PVK/polymer/Ba/Al.

homopolymer. The shape and peak position of EL emission are almost the same as the PL spectra in the solid state (Figure 2a, 3a, and 4). As PL emission in thin film, fluorene emission of EL device was completely quenched for copolymer with the narrow-band-gap monomers loading as low as 1%. EL emission consists exclusively of emission from SeBT or SeBSe units. With increasing SeBT content, EL peaks are also red shifted from 667 nm for PFO−SeBT1 to 708 nm for PFO−SeBT50. For PFO−SeBSe copolymers, the emission peak was moved from 723 nm for PFO−SeBSe1 to 790 nm for PFO−SeBSe15. This fact seems to indicate that the energy-transfer process bears the same mechanism and the recombination zone is the same for both PL and EL processes. The fact that the incorporation of only 1% narrow-band-gap units into copolymer chain completely depresses both the fluorene host emission (λ_{max} = 439 nm) and the wide excimer emission (λ_{max} = 500 nm) (Figure 4) indicates that an intrachain energy trapping process (from fluorene segment to SeBT or SeBSe unit) must be very fast and intrachain energy transfer should be more efficient than interchain interaction between fluorene segments in the polymer aggregates. This indicates again that intramolecular energy transfer plays the major role in devices from such copolymers.

The device performance is summarized in Table 5. All the devices were tested under a fixed current density of 40 mA·cm^{-2} for the convenience of comparison. The external quantum efficiency of the device for PFO−SeBT5 reaches 0.81% at an emission peak ca. 676 nm with PVK as the hole transport layer. When PEDT was used, the device efficiencies are much lower. This is very consistent with the HOMO levels of these copolymers (Table 2). As indicated by the CV measurement (Table 2), the HOMO level of PFO−SeBT and SeBSe copolymers is estimated at around 5.6−5.8 eV toward the vacuum level. Since PEDT has a work function around 4.8−5.0 eV,[32] a significant barrier for hole injection for the device with PEDT anode interlayer exists. Insertion of PVK interlayer (work function 5.6−5.8 eV) significantly improves hole injection in such devices. As can be seen from Table 5, the external quantum efficiencies of the devices for PFO−SeBSe copolymers were lower than those from the corresponding PFO−SeBT copolymers. This is probably related with the fact that the PL efficiencies of PFO−SeBSe copolymers are much lower

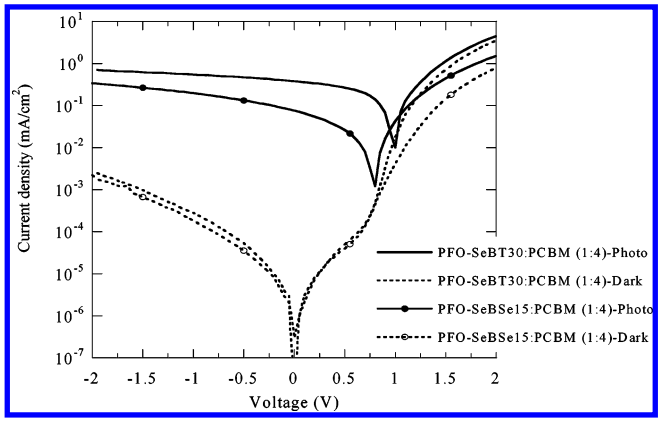

Figure 5. $I-V$ curves of the ITO/PEDT/polymer:PCBM(1:4)/Ba/Al cells under 78.2 mW/cm^2 AM1.5 illumination and in the dark.

Table 6. The Optimized Performances of PVCs for PFO−SeBT:PCBM and PFO−SeBSe:PCBM Blend

active layer	J_{sc} (mA/cm^2)	V_{oc} (V)	*FF* (%)	ECE (%)
PFO-SeBT30:PCBM = 1:4	2.53	1.00	37.4	1.0
PFO-SeBSe15:PCBM = 1:4	0.51	0.80	23.3	0.1

than that of PFO−SeBT. Efforts for further improvement of the device efficiency and further extension of the emission to the longer near-infrared region for PFO−SeBSe are underway.

Characteristics of Photovoltaic Devices. Bulk−heterojunction photovoltaic cells (PVC) were made from copolymers, PFO−SeBT or PFO−SeBSe as the donor phase blending with PCBM as the acceptor phase. Since the optical band gaps of the two narrow-band-gap units, SeBT and SeBSe, were ca. 1.87 and 1.77 eV and absorption peaks corresponding to SeBT and SeBSe were 563 and 605 nm, respectively, we can expect that the spectral response will shift to the deep-red region. Solar cells were fabricated with a sandwich configuration of ITO/PEDT:PSS/PFO−SeBT(or PFO−SeBSe):PCBM/Ba/Al. Table 6 lists the PVC device performance for blend composition, PFO−SeBT30(or PFO−SeBSe15):PCBM = 1:4. The best device performance was obtained for the device from PFO−SeBT30:PCBM (1:4), reaching J_{sc} (short-circuit current) = 2.53 mA/cm^2, V_{oc} (open-circuit voltage) = 1.00 V, and ECE = 1.0% under AM1.5 illumination (78.2 mW/cm^2). We note that the V_{oc} of these devices is around 1.0 V, which is 0.20 V higher than that of PFO−SeBSe/PCBM and also MEH−PPV/PCBM (0.80 V)[33] cells. Since the PCBM:PFO−SeBT ratio, anode interlayer (PEDT), and cathode material (Ba/Al) were the same for the devices listed in the Table 6 and in ref 33, the observed V_{oc} (Figure 5) increase over MEH−PPV:PCBM and PFO−SeBSe/PCBM devices must be related with interfacial properties of PFO−SeBT in the anode and/or acceptor interfaces.

Figure 6 compares the spectral response (normalized) of three devices. Photosensitivity response curves of the devices coincide with the absorption profiles of the corresponding copolymers (Figure 1). Spectral responses of the devices from PFO−SeBSe copolymers are around 750 nm, while that for PFO−SeBT devices is around 675 nm. However, the energy conversion efficiency of PFO−SeBSe devices is lower than that of PFO−SeBT devices (Table 6). Since the active layer of the device are of the same thickness, a much smaller absorption constant of the SeBSe unit in the copolymer than that of PFO−SeBT is probably the main origin of this

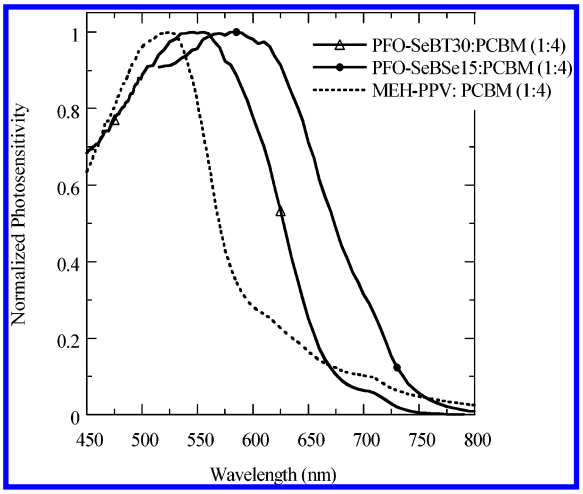

Figure 6. Spectral responses of the ITO/PEDT/polymer:PCBM (1:4)/Ba/Al cells at zero bias.

difference (Figure 1a and c). We also note that somehow the fill factor (*FF*) for PFO−SeBSe devices is systematically lower than that for PFO−BSeT devices. Efforts to optimize the device performance are in progress and will be reported elsewhere.

Conclusion

We synthesized a novel series of fluorene-based copolymers with various molar ratios of narrow-band-gap comonomers, SeBT or SeBSe, of low optical band gaps (E_g = 1.87 eV for SeBT and 1.77 eV for SeBSe, respectively). The efficient and fast energy transfer due to exciton confinement on narrow-band-gap sites has been observed. The PL and EL emissions from the fluorene segment were completely quenched at very low narrow band-gap unit content (1%). The PL and EL efficiencies decreased gradually with increasing the narrow-band-gap unit content, probably due to the heavy Se atom effect. The EL emission peak of the device fabricated from PFO−SeBSe15 shifts to the near-infrared region, around 790 nm. This is the first report of an electroluminescent NIR polymer which contains no rare-earth ions or dye ions. High-performance photovoltaic cells with extended spectral response and increased open-circuit voltage have been achieved from a composite thin film of PFO−SeBT copolymer and PCBM blend.

Acknowledgment. This work was supported by research grants from Ministry of Science and Technology, China (MOST) (#2002CB613402), and National Natural Science Foundation of China (NSFC#50433030).

References and Notes

(1) (a) Burroughes, J. H.; Bradley, D. D. C.; Brown, A. R.; Marks, R. N.; Mackay, K.; Friend, R. H.; Burns, P. L.; Holmes, A. B. *Nature (London)* **1990**, *347*, 539. (b) Ziemelis, K. *Nature (London)* **1999**, *399*, 408. (c) Heeger, A. J. *Solid State Commun*. **1998**, *107*, 673. (d) Sugura, J. L. *Acta Polym*. **1998**, *49*, 319.

(2) (a) Kraft, A.; Grimsdale, A. C.; Holmes, A. B. *Angew. Chem., Int. Ed*. **1998**, *37*, 402. (b) Bernius, M. T.; Inbasekaran, M.; O'Brien, J.; Wu, W. *Adv. Mater*. **2000**, *12*, 1737.

(3) Kim, D. Y.; Cho, H. N.; Kim, C. Y. *Prog. Polym. Sci*. **2000**, *25*, 1089.

(4) (a) Doi, S.; Kuwabara, M.; Noguchi, T. *Synth. Met.* **1993**, *57*, 4174. (b) Johansson, D. M.; Srdanov, G.; Yu, G.; Theander, M.; Inganas, O.; Anderson, M. R. *Macromolecules* **2000**, *33*, 2525.

(5) (a) Rehahn, M.; Schluter, A.; Wegner, G.; Feast, W. J. *Polymer* **1989**, *30*, 1054. (b) Yang, Y.; Pei, Q.; Heeger, A. J. *J. Appl. Phys.* **1996**, *79*, 934.
(6) (a) Pei, J.; Yu, W. L.; Ni, J.; Lai, Y. H.; Huang, W.; Heeger, A. J. *Macromolecules* **2001**, *34*, 7241. (b) Groenendaal, L. B.; Jonas, F.; Freitag, D.; Pielartzik, H.; Reynolds, J. R. *Adv. Mater.* **2000**, *12*, 482.
(7) (a) Fukuda, M.; Sawada, K.; Yoshino, K. *J. Polym. Sci., Part A: Polym. Chem.* **1993**, *31*, 2465. (b) Pei, Q.; Yang, Y. *J. Am. Chem. Soc.* **1996**, *118*, 7416. (c) Kameshima, H.; Nemoto, N.; Endo, T. *J. Polym. Sci., Part A: Polym. Chem.* **2001**, *39*, 3143. (d) Scherf, U.; List, E. J. W. *Adv. Mater.* **2002**, *14*, 477.
(8) Leclerc, M. *J. Polym. Sci., Part A: Polym. Chem*. **2001**, *39*, 2867.
(9) Inbasekaran, M.; Woo, E. P.; Wu, W. S.; Bernius, M. T. PCT application, WO 00/46321A1, 2000.
(10) Hou, Q.; Xu, Y.; Yang, W.; Yuan, M.; Peng, J.; Cao, Y. *J. Mater. Chem.* **2002**, *12*, 2887.
(11) Yang, R.; Tian, R.; Yang, W.; Hou, Q.; Cao, Y. *Macromolecules* **2003**, *36*, 7453.
(12) Yang, J.; Jiang, C.; Zhang, Y.; Yang, R.; Yang, W.; Hou, Q.; Cao, Y. *Macromolecules* **2004**, *37*, 1211.
(13) Suzuki, H.; Yokoo, A.; Notomi, M. *Polym. Adv. Technol.* **2004**, *15*, 75.
(14) Suzuki, H. *Appl. Phys. Lett.* **2000**, *76*, 1543.
(15) (a) Hebbink, G. A.; Stouwdam, J. W.; Reinhoudt, D. N.; van Veggel, F. C. J. M. *Adv. Mater.* **2002**, *14*, 1147. (b) Slooff, L. H.; Polman, A.; Cacialli, F.; Friend, R. H.; Hebbink, G. A.; van Veggel, F. C. J. M.; Reinhoudt, D. N. *Appl. Phys. Lett*. **2001**, *78*, 2122. (c) Tessler, N.; Medvedev, V.; Kazes, M.; Kan, S.; Banin, U. *Science* **2002**, *185*, 1906.
(16) Brabec, C. J.; Winder, C.; Sariciftci, N. S.; Hummelen, J. C.; Dhanabalan, A.; van Hal, P. A.; Janssen, R. A. J. *Adv. Funct. Mater*. **2002**, *12*, 709.
(17) (a) Woo, E. P.; Inbasekaran, M.; Shiang, W.; Roof, G. R. WO 97/05184, 1997. (b) Lee, J. I.; Klaerner, G.; Miller, R. D. *Chem. Mater*. **1999**, *11*, 1083.
(18) Ranger, M.; Rondeau, D.; Leclerc, M. *Macromolecules* **1997**, *30*, 7686.
(19) Pilgram, K.; Zupan, M.; Skiles, R. *J. Heterocycl. Chem*. **1970**, *7*, 629.
(20) Tsubata, Y.; Suzuki, T.; Miyashi, T.; Yamashita, Y. *J. Org. Chem*. **1992**, *57*, 6749.
(21) Pinhey, J. T.; Roche, E. G. *J. Chem. Soc., Perkin Trans. 1* **1988**, 2415.
(22) Kitamura, C.; Tanaka, S.; Yamashita, Y. *Chem. Mater*. **1996**, *8*, 570.
(23) Inbasekaran, M.; Wu, W. S.; Woo, E. P. U.S. Patent 5,777,-070, 1998.
(24) Yang, X.; Yang, W.; Yuan, M.; Hou, Q.; Huang, J.; Zeng, X.; Cao, Y. *Synth. Met*. **2003**, *135*−*136*, 189.
(25) Janietz, S.; Bradley, D. D. C.; Grell, M.; Giebeler, C.; Inbasekaran, M.; Woo, E. P. *Appl. Phys. Lett.* **1998**, *73*, 2543.
(26) de Leeuw, D. M.; Simenon, M. M. J.; Brown, A. R.; Einerhand, R. E. F. *Synth. Met*. **1997**, *87*, 53.
(27) Yang, W.; Huang, J.; Liu, C.; Niu, Y.; Hou, Q.; Yang, R.; Cao, Y. *Polymer* **2004**, *45*, 865.
(28) Gong, X.; Moses, D.; Heeger, A. J.; Xiao, S. *Synth. Met.* **2004**, *141*, 17.
(29) Gong, X.; Moses, D.; Heeger, A. J.; Xiao, S. *J. Phys. Chem. B* **2004**, *108*, 8601.
(30) Berggren, M.; Gustafsson, G.; Inganas, O.; Andersson, M. R.; Wennerstrom, O.; Hjertberg, T. *Appl. Phys. Lett*. **1994**, *65*, 1489.
(31) Baigent, D. R.; Hamer, P. J.; Friend, R. H.; Moratti, S. C.; Holmes, A. B. *Synth. Met*. **1995**, *71*, 2175.
(32) Cao, Y.; Yu, G.; Zhang, C.; Menon, R.; Heeger, A. J. *Synth. Met*. **1997**, *87*, 171.
(33) Deng, X.; Zheng, L.; Yu, G.; Mo, Y.; Yang, W.; Wu, T.; Cao, Y. *Chinese J. Polym. Sci.* (*Engl.*) **2001**, *19*, 597.

MA047969I